



A Model of Visuospatial Working Memory in Prefrontal Cortex: Recurrent Network and Cellular Bistability

MARCELO CAMPERI

*Center for Complex Systems, Brandeis University, Waltham, MA 02254; Physics Department,
University of San Francisco, San Francisco, CA 94117*

camperi@lynx.cs.usfca.edu

XIAO-JING WANG

Center for Complex Systems and Department of Physics, Brandeis University, Waltham, MA 02254

xjwang@volen.brandeis.edu

Received July 11, 1997; Revised January 14, 1998; Accepted January 26, 1998

Action Editor: Richmond

Abstract. We report a computer simulation of the visuospatial delayed-response experiments of Funahashi et al. (1989), using a firing-rate model that combines intrinsic cellular bistability with the recurrent local network architecture of the neocortex. In our model, the visuospatial working memory is stored in the form of a continuum of network activity profiles that coexist with a spontaneous activity state. These neuronal firing patterns provide a population code for the cue position in a graded manner. We show that neuronal persistent activity and tuning curves of delay-period activity (memory fields) can be generated by an excitatory feedback circuit and recurrent synaptic inhibition. However, if the memory fields are constructed solely by network mechanisms, noise may induce a random drift over time in the encoded cue position, so that the working memory storage becomes unreliable. Furthermore, a “distraction” stimulus presented during the delay period produces a systematic shift in the encoded cue position. We found that the working memory performance can be rendered robust against noise and distraction stimuli if single neurons are endowed with cellular bistability (presumably due to intrinsic ion channel mechanisms) that is conditional and realized only with sustained synaptic inputs from the recurrent network. We discuss how cellular bistability at the single cell level may be detected by analysis of spike trains recorded during delay-period activity and how local modulation of intrinsic cell properties and/or synaptic transmission can alter the memory fields of individual neurons in the prefrontal cortex.

Keywords: working memory, prefrontal cortex, bistability, network attractor dynamics

Introduction

Working memory is the distinct memory ability of humans and animals to retain information in temporal storage and manipulate it “online,” usually for a short time span of seconds. It subserves to “mediation of cross-temporal contingencies” (Fuster, 1988), which is indispensable for such cognitive tasks as performing

a sequence of motor movements, planning, or comprehending a written sentence.

The prefrontal cortex (PFC) plays a preeminent role in the working memory processes of all sensory modalities. This has been demonstrated by converging evidence from lesion and brain cooling studies (Fuster, 1988; Goldman-Rakic, 1987), as well as PET scans (Petrides et al., 1993; Haxby et al., 1995) and fMRI

imaging (McCarthy et al., 1994; Cohen et al., 1997; Courtney et al., 1997). Neuronal correlates of working memory have been documented by electrophysiological studies, using single-unit recordings from an awake monkey's PFC during delayed-response tasks. In these experiments, between a sensory cue and the behavioral response, some PFC neurons were found to exhibit enhanced firing activity that persisted across the entire delay period after the removal of the sensory input (Fuster and Alexander, 1971; Kubota and Niki, 1971; Funahashi et al., 1989; Goldman-Rakic, 1995). Presumably, during the delay period (typically of a few seconds), information specific to the sensory stimulus is being encoded and actively held online in the form of PFC neural network firing patterns. This information is then read out by downstream neural systems at the "go" signal and used by the animal to carry out the required behavioral response.

In a particularly well-controlled oculomotor delayed-response experiment (Funahashi et al., 1989), a monkey is trained to keep its gaze on a light spot at the center of a monitor. A cue light spot is shown to the monkey transiently for 0.5 s, at one of eight equidistant positions (in a random sequence) on a circle centered at the fixation spot. This fixation signal is present during the whole delay period (3 to 5 s) that follows the suppression of the cue input. After this delay, the fixation spot is turned off. This constitutes the go signal for the monkey, who has then to saccade toward the original position of the cue. Since anticipatory responses and other possible causes of the sustained activity (such as motor-related activity) are discarded, correct performance is possible only based on an actual recall of the cue position (Funahashi et al., 1989). In this study, neurons in the principal sulcal region (PS) were found to exhibit persistent delay-period activity. This activity was interpreted as a mnemonic coding for the position of the original stimulus (the cue) in the monkey's visual field. Moreover, it was shown in Funahashi et al. (1989) that some PFC neurons have *memory fields*—namely, a neuron shows strong persistent activity during the delay period only when the cue is close to a particular location in the visual field (say θ , corresponding to a preferred position on the cue circle). A *tuning curve* of a PFC cell is then defined as the mean firing rate during the delay period as function of the cue position. Such a curve shows a maximum at the preferred position θ and a minimum (which is normally lower than the spontaneous firing rate of the cell) at the cue position 180 degrees away from θ (Funahashi et al., 1989; Goldman-Rakic, 1995).

The PFC local circuitry underlying persistent firing patterns remains not well understood. Goldman-Rakic (1995) has proposed a network wiring scheme with recurrent excitation and lateral inhibition, which would underlie the formation of the memory fields of the dorsolateral PFC neurons. Horizontal connections are a salient feature of cortical circuits (Douglas et al., 1991; Gilbert 1993), and recurrent network models have been proposed to underlie various kinds of cortical tuning computation (Somers et al., 1995; Ben-Yishai et al., 1995; Stemmler et al., 1995; Salinas and Abbott, 1996; Lukashin et al., 1996; Zhang, 1996; Ben-Yishai et al., 1997). In contrast to these examples, in order to perform a working memory rather than a purely sensory or motor function the PFC network should be able to be "switched on" into a persistent firing pattern by *transient* cue stimuli and be "turned off" back to its resting state of spontaneous activity by a suitable "go" signal. Early theoretical modeling works have shown that a recurrent neural network may be capable of displaying under equal conditions either a uniform rest state or an excited state with a nonuniform spatial profile of neuronal activity (Wilson and Cowan, 1973; Amari, 1977). This *bistability* phenomenon, solely originated in the network circuit, provides a candidate mechanism for sustained neuronal representation of sensory stimuli that can be turned on by transient inputs.

Other modeling works have hypothesized that *single* PFC neurons could be bistable and could be switched on and off by synaptic inputs (Guigon et al., 1995). By cellular bistability we mean the ability of a single neuron to possess two stable membrane states corresponding to different activation conditions of various voltage-dependent ionic currents. For instance, a neuron can be either in a spontaneous low-rate firing state or in an excited state if a certain plateau potential is switched on by transient input perturbations. (For an explanation and examples from vertebrate and invertebrate motoneurons, see Kiehn, 1991, and Marder et al., 1996, respectively). Typically, neuromodulatory inhibition of certain output potassium currents is required to unmask the plateau potential and enable the bistability behavior. Recent *in vitro* rat PFC slice experiments revealed that PFC neurons are endowed with a multitude of voltage-gated ion channels, including persistent Na^+ channel (Gejjo-Barriento and Pastore, 1995), slowly inactivating K^+ channel (Hammond and Crépel, 1992), high-threshold Ca^{2+} channels located at the dendritic sites (Yang et al., 1996), and Ca^{2+} -activated non-selective cation channels (Haj-Dahmane and Andreda, 1996). Computer simulations have shown that both

persistent Na^+ current (Steinberg, 1988) and dendritic high-threshold Ca^{2+} currents (Booth and Rinzel, 1995; Booth et al., 1997) are capable of producing a plateau potential giving rise to neuronal bistability. Therefore, although there is yet no evidence that mammalian (primate in particular) PFC neurons may become bistable (for example, under specific neuromodulatory influences), it is of interest to consider how cellular bistability may contribute to the formation of memory fields of PFC neurons.

In this work, we present a neural network computer simulation of the oculomotor delayed-response experiment of Funahashi et al. (1989). We assume that the visuospatial persistent activity is generated locally in a module of the dorsolateral PFC near the principal sulcus, and our model combines recurrent network synaptic mechanisms (Goldman-Rakic, 1995) with intrinsic cellular bistability. Our main objective is to assess how the interplay between single neuron properties (bistability) and network circuits can reproduce the main experimental observations, especially the tuning curves of delay-period activity (neuronal memory fields). In our model, the working memory of the cue stimulus position is assumed to be coded by a persistent activity profile distributed across the neural population. In fact, there should be a continuum of stable, nonuniform activity profiles, which can be used to encode any cue position in a graded manner. These nonuniform activity profiles are steady states of the model. In addition, there is also another steady state—a uniform, stable rest state, where the whole neuronal population is characterized by a spontaneous firing at low rates. In the absence of any external input, the network will choose the rest state. The transient cue and the subsequent go signal act as the switches between the rest state and one of the active states. We also show that memory fields may be formed solely by recurrent network circuits, without cellular bistability. In that case, however, the working memory storage is not robust against noise or distraction inputs.

A brief report of the present work has appeared in Camperi and Wang (1997).

Methods

Single-Neuron Bistability

The activity of a single neuron is modeled by its firing rate r , which obeys the following dynamical

equation:

$$\tau_0 \frac{dr}{dt} = -f(r) + g(I), \quad (1)$$

where τ_0 is a characteristic time of the cell and I is the total input. The function $f(r)$ and the gain $g(I)$ represent the intrinsic properties of the neuron. In order to guarantee that the firing rate is always positive, $g(I)$ (Fig. 1B) is taken to be $g(I) = I$ if I is larger than a threshold and zero otherwise (actually, the threshold is normally set to be zero).

For convenience, we consider r and $f(r)$ as *dimensionless* by assuming $r = \hat{r}/\hat{r}_0$, where \hat{r} is the actual firing rate of the neuron (in Hz) and \hat{r}_0 is a reference firing rate. We used $\hat{r}_0 = 7$ Hz, so that in the *network* model (see below), the neuronal spontaneous firing rate is about 3 to 5 Hz, comparable to the measurements from dorsolateral PFC neurons (Funahashi et al., 1989). In addition, we used $\tau_0 = 25$ ms. Both τ_0 and \hat{r}_0 are fixed throughout the article. The particularly chosen values do not affect the qualitative behavior of the model.

The steady state of this system is obtained by setting $dr/dt = 0$ in Eq. (1)—namely, by solving the equation $f(r) = g(I) = I$ (assuming I is above the threshold). Thus, $r = f^{-1}(I)$ (where f^{-1} is the inverse function of f) constitutes the neuronal input-output relation. The neuron is bistable if this relation displays an S-shape curve, as shown in Fig. 1A. In this case, there is a range of input amplitudes, $I_1 < I < I_2$, for which the cell can be in either one of two possible steady states, corresponding to a low (spontaneous) and high (activated) firing rate, respectively. The bistability can be realized if $f(r)$ is not linear but cubic in r , like

$$f[r] = c + r - ar^2 + br^3, \quad (2)$$

where the parameters $a = 0.36$, $b = 0.038$, and $c = -0.2$ were used for Fig. 1A. The input range of the *bistable* regime ($I_2 - I_1$) and the gap between the spontaneous and excited activity levels ($r_+ - r_-$) are controlled by the parameters a and b . In the Results section, we discuss how the network behavior depends on the values chosen for these parameters. Moreover, as illustrated in Fig. 1C, switching between the two states can be induced by transient inputs. Note that in this model, the bistable behavior is not possible without a baseline input drive I between I_1 and I_2 . In the network model, such a tonic drive originates from

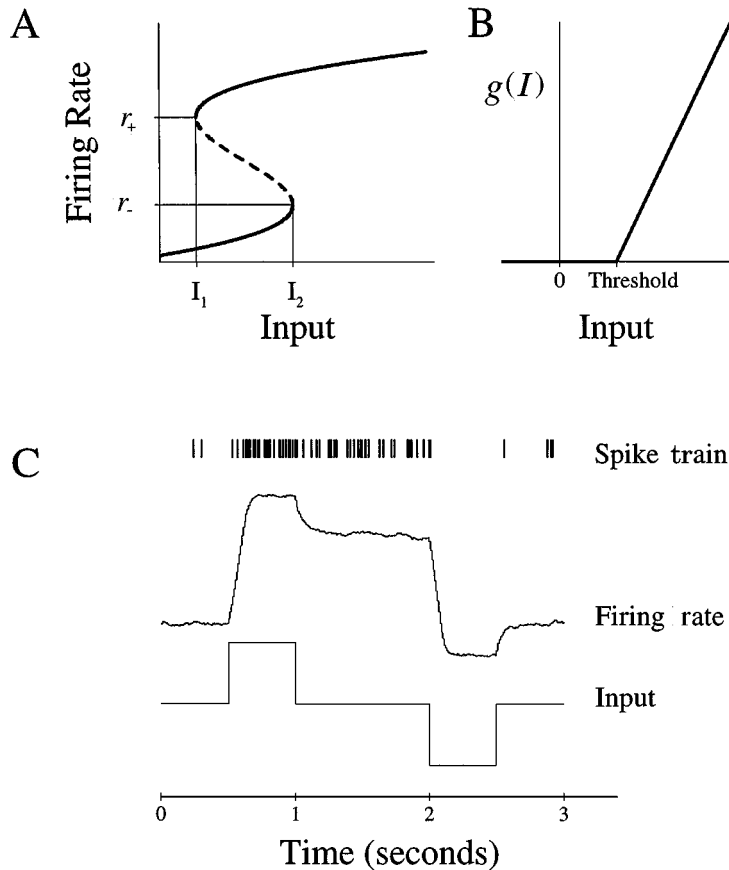


Figure 1. A: Input-output relation for a bistable neuron (solid lines: stable states, dashed line: unstable states), obtained using $f(r)$ as a cubic function of r (Eq. (2)). For the parameters used in this work, r_+ and r_- correspond to firing rates of 29.75 and 14.42 Hz, respectively. Note that the model neuron's bistability is *conditional* and requires a sustained input of an appropriate amplitude between $I_1 = 0.46$ and $I_2 = 0.66$. B: The gain function $g(I)$. C: Simulation (with white noise added) of the neuron in A. Plotted are (bottom to top panels) transient input pulses, firing rate $r(t)$, and sample spike train (generated by a Poisson process with rate $r(t)$). The baseline input ($I = 0.5$) corresponds to a value in between I_1 and I_2 , with transient pulses of amplitude ± 0.5 . The average firing rates in the lower and upper states are approximately 7.5 and 42.5 Hz, respectively. Note that these firing rates are not the actual rest and excited firing rates of neurons in a network, which depend on recurrent excitatory and inhibitory synaptic interactions.

reverberating synaptic inputs through recurrent excitatory connections, which are activated only by some stimulus. In this sense, a single neuron is assumed to be only a *conditional* bistable device.

Network Model

We use a simple model that captures the relevant architectural organization of local cortical circuits. It is adapted from a model of orientation selectivity in a hypercolumn of primary visual cortex (Ben-Yishai et al., 1995). The network consists of N neurons (typically $N = 50 - 200$), each labeled by its preferred

cue location or memory field θ . This parameter ranges from $-\pi$ to π , along a circle.

In the large network limit, we can assume that the neurons cover uniformly all the angles. In this limit, the firing rate $r(\theta, t)$ of the cell with memory field in the neighborhood of θ and at time t obeys the following mean-field equation:

$$\tau_0 \frac{d}{dt} r(\theta, t) = -f[r(\theta, t)] + g[I(\theta, t)] + \sigma \eta(t), \tag{3}$$

where we have assumed that all neurons are identical and exhibit conditional bistability in $f(r)$ given by

Eq. (2). The second term, $g[I(\theta, t)]$, is the synaptic drive. The third term, $\sigma\eta(t)$, is a white-noise input, which is uncorrelated between cells. The total input current to each neuron I is the sum of an external input I^{ext} for the transient cue and the go signal, and a recurrent synaptic input that is the product of the coupling strength W and the presynaptic firing rate (summed over all presynaptic cells). Thus, the input I to the neuron with memory field θ is represented by the following equation:

$$I(\theta, t) = I^{\text{ext}}(\theta, t) + \int_{-\pi}^{\pi} \frac{d\theta'}{2\pi} W(\theta - \theta') r(\theta', t), \quad (4)$$

where $W(\theta - \theta')r(\theta', t)$ is the input from the presynaptic cell at θ' to the postsynaptic cell at θ and the integral represents the summation over all presynaptic cells. The interaction W between two neurons includes a global inhibition and a structured excitation that depends on the difference of their respective memory fields, $\theta - \theta'$. It is given by (cf. Fig. 2)

$$W(\theta) = -W_I + W_E \left(\frac{1 + \cos \theta}{2} \right)^q. \quad (5)$$

Here, the constants W_I and W_E represent the strengths of the inhibitory and excitatory interactions, respectively. Notice that the modulation function, $(1 + \cos \theta)/2$ (with q controlling its width), was chosen for its simplicity. Other reasonable periodic functions would work as well. Furthermore, the external input $I^{\text{ext}}(\theta, t)$ contains a constant bias input I_0 and a cue stimulus. It is given by

$$I^{\text{ext}}(\theta, t) = I_0 + I_{\text{cue}} \left(\frac{1 + \cos(\theta - \theta_0)}{2} \right)^p, \quad (6)$$

where the constant I_{cue} is nonzero only during the transient cue stimulus—say, starting at t_0 and lasting for a time $\Delta t = 500$ ms. The modulation function, similar to that used in Eq. (5), peaks at θ_0 , and thus represents a cue centered at $\theta = \theta_0$ (again, the actual form is irrelevant, as long as it is strong enough and modulated with a peak at the cue location). Since it is not known how the persistent activity in PFC neurons is turned off at the end of the delay period, we did not model it explicitly. The go signal was then simulated with a uniform inhibitory input to all the neurons. Unless specified otherwise, the parameter values used are $W_E = 2.6$, $W_I = 2.0$, $I_0 = 0.45$, $p = q = 1$, and $I_{\text{cue}} = 1$.

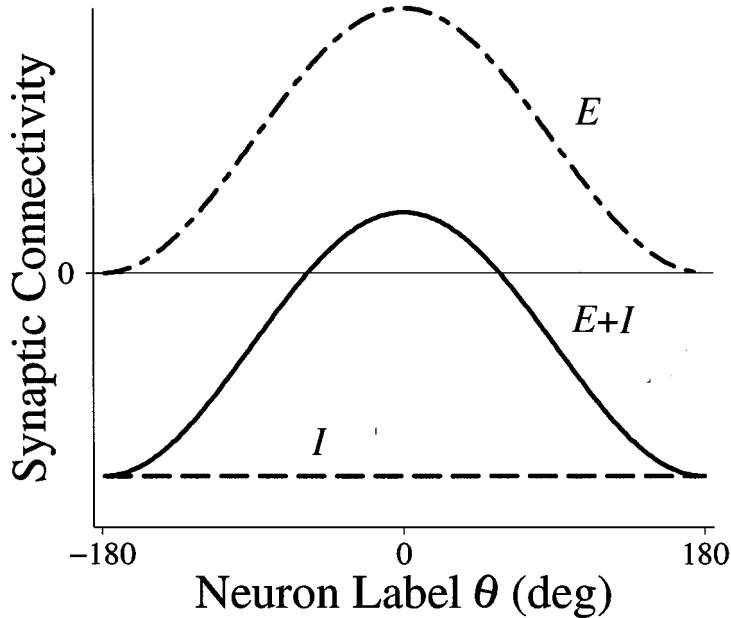


Figure 2. Synaptic connectivity of the network model, given by Eq. (5). The curves E and I represent, respectively, the excitatory and inhibitory coupling strengths from the presynaptic neuron at $\theta = 0$ to postsynaptic neurons located at any θ . The net synaptic effect ($I + E$) is excitatory to nearby neurons and inhibitory to distal neurons.

Population Vector

In our model, the memory of the cue is coded by the peak of the network activity profile. However, in the presence of noise, the neuronal firing pattern in the network fluctuates over time, and it is no longer clear where the peak is located. To read out the memorized cue position for delay-period activity, we used a *population vector* (Georgopoulos et al., 1986), which involves a vectorial average across neurons in the network with weights given by their instantaneous firing rates $r(\theta)$. Specifically, each angular value θ corresponds to a unit vector $(\cos \theta, \sin \theta)$ on the circle. Given a discrete profile of neural activities $r(\theta_i, t)$ in the network, the population vector (v_x, v_y) is given by the weighted sum of individual unit vectors:

$$(v_x, v_y) = \left(\sum_i r(\theta_i, t) \cos \theta_i, \sum_i r(\theta_i, t) \sin \theta_i \right). \quad (7)$$

Let us write

$$(v_x, v_y) = v (\cos \theta_{\text{peak}}, \sin \theta_{\text{peak}}), \quad (8)$$

where $v = \sqrt{v_x^2 + v_y^2}$ is the length of the vector (v_x, v_y) . Then, the orientation of the population vector, given by

$$\theta_{\text{peak}} = \tan^{-1} \left(\frac{v_y}{v_x} \right), \quad (9)$$

is the cue location encoded by the distributed neuronal activity pattern in the network.

Results

An example of the model simulation is shown in Fig. 3. After the network settles into a uniform rest state with spontaneous firing rate of about 5 Hz, a cue input (Eq. (6)) is presented transiently. A network activity profile is thus generated that outlasts the cue stimulus. The persistent activity profile is unique and largely determined by recurrent excitatory and inhibitory connections. Hence, it does not depend on the details of the input; in particular, it is considerably narrower than the chosen input cue profile (Fig. 3). The persistent activity can be turned off by an inhibitory go signal. Note that for any amplitude of this negative input, the

actual drive to neurons cannot be smaller than zero, due to the gain function $g(I)$.

The working memory of the cue stimulus is thus encoded in the form of this network activity profile, which peaks at the location of the original cue (Fig. 4A). This behavior is partly due to the cellular bistability of single neurons in the network: those neurons that receive sufficiently large inputs during the cue stimulus are driven to jump to the upper activity level on their input-output relation curve (Fig. 1A). However, they are sustained in the excited state only by the recurrent excitation in the network, without which the total inputs to those cells would have been below I_1 (cf. Fig. 1A), and thus neurons would not be able to stay active after the cue is turned off. The network model presents a continuum of possible steady-state activity profiles such as that in Fig. 4A, each centered at a different θ location. Such states are called *marginal states* (Ben-Yishai et al., 1995; Zhang, 1996). A particular profile is selected by the cue input location. The shape of all the nonuniform activity profiles is unique; its width being delimited by the number of cells whose synaptic inputs exceed I_1 (Fig. 4B). The remaining cells with synaptic input below I_1 stay inactive during delay period; in fact, their firing rates are *decreased* compared to the spontaneous rate because they receive lateral inhibitory inputs from the activated cells. This effect has been seen experimentally (Funahashi et al., 1989). The feedback inhibition is crucial in generating a nonuniform activity profile (hence, a tuning curve for individual cells, as we shall see below).

Experimentally recorded spike trains of persistent delay-period activity appear to be quite noisy (Fuster and Alexander, 1971; Funahashi et al., 1989; Goldman-Rakic, 1995), and we included this effect in the simulations by the addition of white noise in Eq. (3). A spatial activity profile can be obtained by averaging over a long period of time, which is equivalent to an average over different trials. In Fig. 4A, we compare the steady-state network profile during the delay period following a cue centered at $\theta = 0^\circ$, without and with white noise. Without noise, there are two gaps in the activity profile. The gaps are caused by a finite jump in the firing rate between the lower and upper branches of the input-output relation (Fig. 1A) and are not related to the number of neurons used in the simulation (they still exist when N goes to infinity). These gaps appear to have been rounded off when noise is present because neurons that are within the bistable regime—namely, with inputs between I_1 and I_2 (cf. Fig. 1A)—are induced to

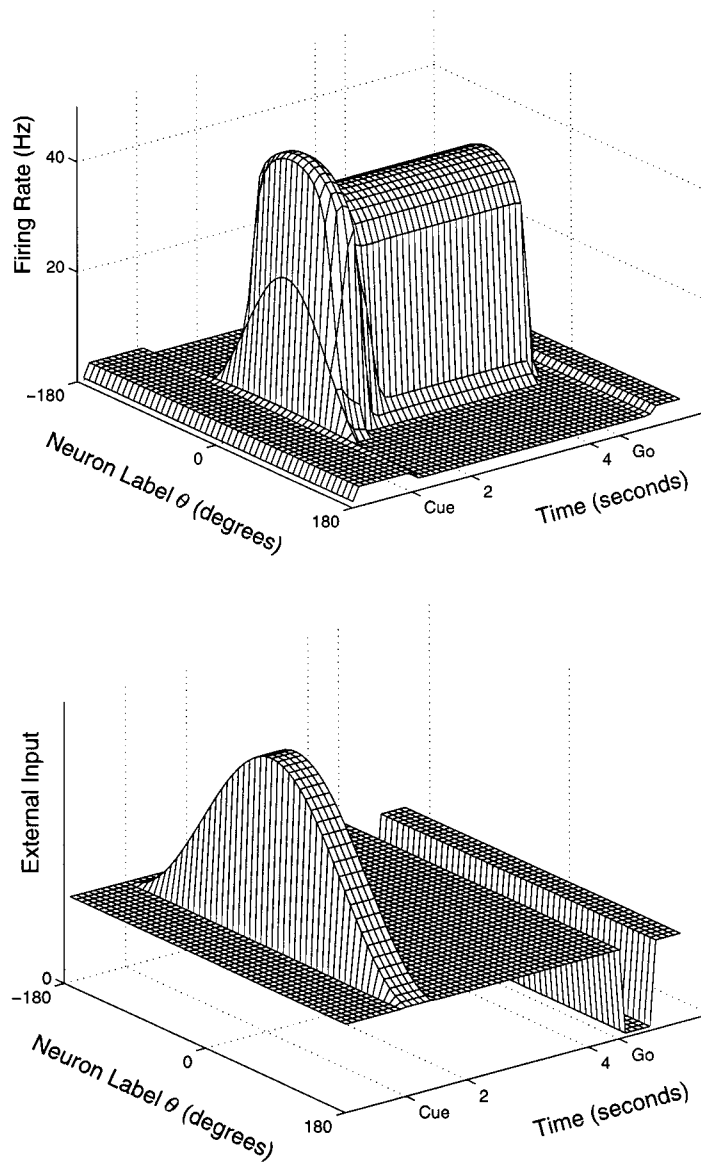


Figure 3. Space-time plots of the network activity (upper panel) and external input (lower panel) for a delayed-response simulation. The persistent network activity profile is triggered by a transient cue stimulus and is switched off by an inhibitory go signal, both lasting for 500 ms. The steady-state activity profile during the delay period is not sensitive to the form of the anisotropic input and is narrower than the input spatial distribution. In addition, note that the firing rate of neurons far away from the peak activity is *decreased* with respect to the spontaneous firing rate. The model parameters are given in the Methods section.

switch between the upper and lower states by virtue of the noise. This is obviously more likely to happen for cells closer to the gaps of the activity profile (whose inputs are closer to I_1). That is, a given cell is expected to display random switching when the cue location is intermediate between its “best” and “worst” stimuli.

Tuning Curve

For a very large number of cue positions, the shape of the spatial activity profile (Fig. 4A) must be the same as that of the tuning curve for an individual neuron, defined as the mean firing rate during the delay period as

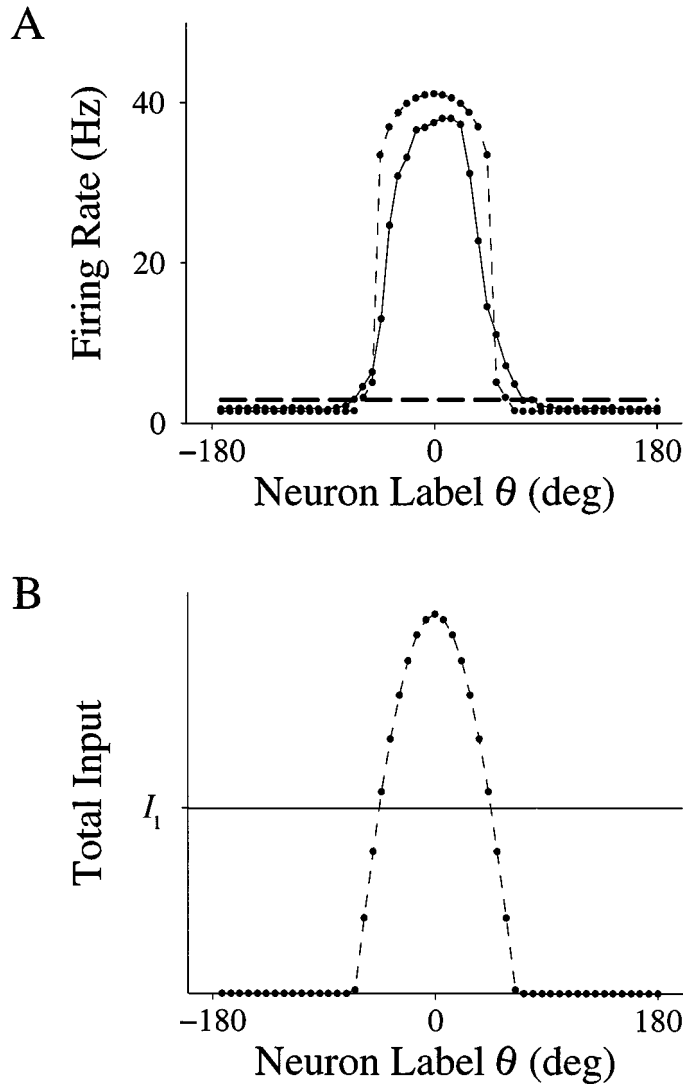


Figure 4. A: Steady-state profile of the persistent network activity during delay period, with and without noise (solid and dashed curves, respectively). Discrete data points were obtained by simulations using a finite number of cells (50 in this case). In the absence of noise, the activity profile displays two (symmetrical) discontinuities, due to a finite gap between bistable levels in the single cell input-output relation (cf. Fig. 1A). With added noise, cells near the discontinuities can switch randomly between the two states, so that the activity profile averaged over long time appears to be smooth. B: Total input profile (constant bias + synaptic) during the delay period. Note that the cells in the up state are those whose total inputs exceed I_1 (cf. Fig. 1A).

function of the input cue location. However, if a small number of cue positions are used, the tuning curve of a given cell will appear to be different. This will also depend on whether any of the presented cue positions coincides with the neuron's memory field or not. We computed tuning curves of single neurons, using eight different input cues located at intervals of 45 degrees, a setup similar to the experiment of Funahashi et al. (1989). Results from such simulation are shown in

Fig. 5, which bears a close similarity with analogous plots in Funahashi et al. (1989).

The tuning curves of two neurons, one with memory field at a cue location and another with memory field in between cues, were calculated in this way (Figs. 6A and 6B, respectively). The data obtained was fitted well by a Gaussian function, using the conventional Marquardt-Levenberg algorithm. The width of the tuning curve calculated this way is 30.89 degrees in Fig. 6A and

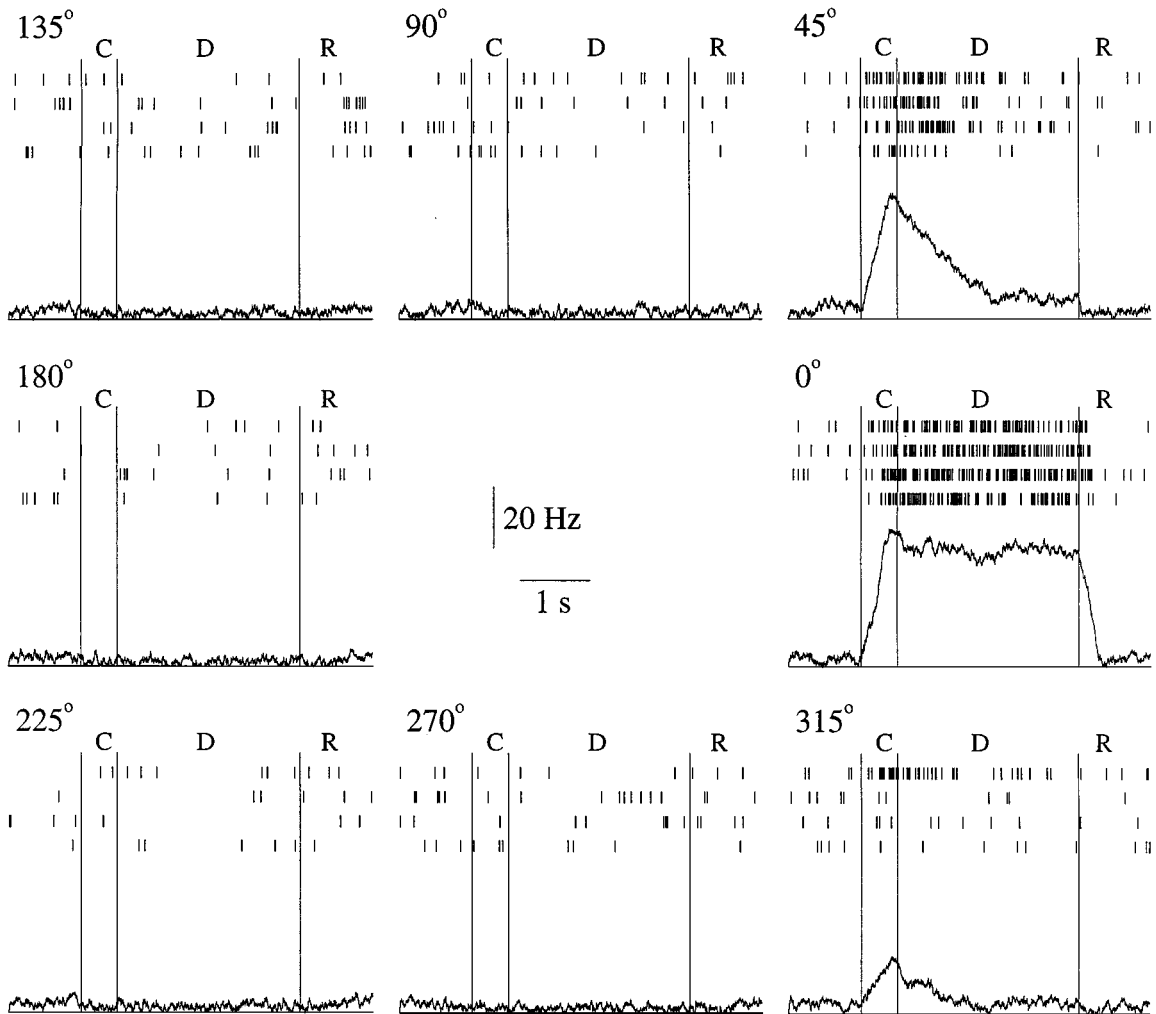


Figure 5. Firing activity of a neuron with memory field centered at $\theta = 0$ degree, when eight cue stimuli are presented at every 45 degrees (indicated at the upper-left corner of each panel). Solid lines: firing rate $r(\theta = 0 \text{ degree}, t)$ averaged over trials (in the presence of noise). Rastergrams for four different trials were produced by a Poisson model of spike generation with rate $r(t)$. The cue stimulus presentation, delay period, and post-go-signal (or response) periods are indicated by C, D and R, respectively.

25 degrees in Fig. 6B. These are comparable with experimentally measured tuning curves of delay period activity of PFC cells (20 to 50 degrees by Gaussian fit, see Funahashi et al., 1989). Indeed, results from these simulations could always be fitted to Gaussian functions with similar widths. The width of the tuning curve depends on the model parameters (see below). In particular, the exponent q in Eq. (5) controls the extent of recurrent excitatory connection, which is a major factor in shaping the activity profile and the tuning curves of single cells.

Note that fitting to a Gaussian function was done only for the practical purpose of direct comparison with the results of Funahashi et al. (1989). In the model, it is not

rigorously correct since we know that if a sufficiently large number of cues is used, the tuning curve of a single cell should look the same as the network activity profile (cf. Fig. 4A), which cannot be fitted by a Gaussian function. Therefore, it would be interesting to compare our model with experimentally measured tuning curves using more than eight cue positions. Furthermore, in principle, a tuning curve should be a periodic function of the cue position θ , while a Gaussian is not.

State Diagrams

Our model exhibits three qualitatively different steady-state behaviors—a uniform Down state, representing

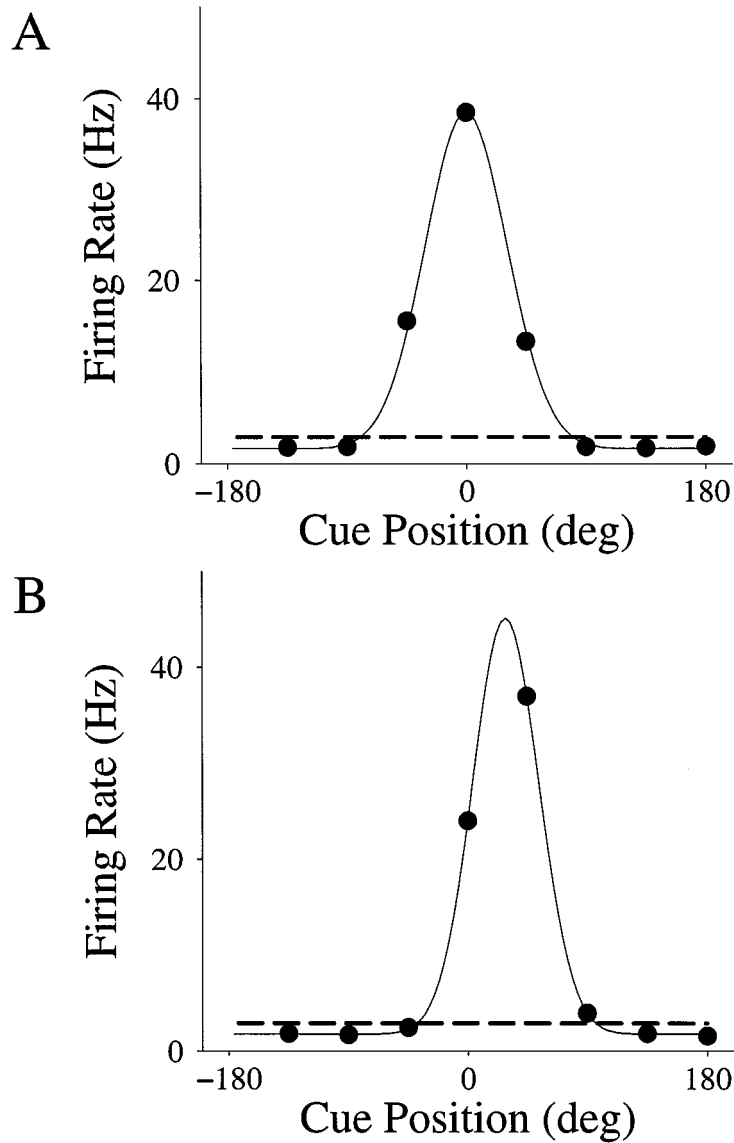


Figure 6. Tuning curves of delay period activity for two neurons (averaged over noise). A: Neuron at $\theta = 0$ degree (which coincides with one of the eight cues). B: Neuron at $\theta \approx 28$ degrees (which is in between presented cues). The solid lines are nonlinear regression fits of the tuning curve data (using the Marquardt-Levenberg algorithm). In both panels, the data fit well to a Gaussian function $G(\theta) = \gamma + \alpha \exp[-(\theta - \delta)^2/2\sigma^2]$, with $\alpha = 36.84$, $\gamma = 1.67$, $\delta = 0$ degree, and $\sigma = 30.89$ degrees for panel A, and $\alpha = 43.25$, $\gamma = 1.82$, $\delta = 28.9$ degrees, and $\sigma = 25$ degrees for panel B. Again, note that the activity level is *decreased* with respect to the spontaneous activity (indicated by the dashed line), when the cues are far away from the memory field of the given neuron.

the rest state with a low spontaneous firing rate $\tilde{r} < r_- \approx 14$ Hz for all θ ; a nonuniform activity Profile state (such as those shown in Figs. 3 and 4), which in fact consists of a continuum of profiles which peak at any θ (“marginal states” due to the spatial translational symmetry of the network); and a uniform Up state, where every neuron fires at a same and high rate

$\tilde{r} > r_+ \approx 30$ Hz (r_- and r_+ as in Fig. 1A). The Up state cannot be used to encode spatial information of a cue position and is more akin to a pathological epileptic behavior. For a given parameter set, some of the three states may not exist or may be unstable. The working memory mechanism of the model is based on a coexistence of a stable rest Down and active Profile states,

where by coexistence we mean that both are possible steady states under the same condition, and the network can be in either of the two states. This requires certain constraints to be satisfied by single neuronal input-output properties as well as circuit connections.

Concerning the single-cell input-output relation (Fig. 1A), there are two limiting cases. First, the single-cell conditional bistability requires this curve to exhibit a sharp S-shape, which, for the given value of b , imposes that a be larger than a critical value $a_1 \simeq 0.3376$. On the other hand, when a is larger than $a_2 \simeq 0.3819$, I_1 becomes negative, which means that even in the absence of any sustained excitation, all neurons can be in either a low or a high firing states: they become “unconditional” bistable devices. Thus, individual neurons would have two possible spontaneous firing rates, which is not observed experimentally. Moreover, if neurons are unconditionally bistable, they are more likely to be switched on by noise, which would create errors in the memory storage of the population-coded cue position. Therefore, the value of a should be limited between a_1 and a_2 , so that single neurons are only conditionally bistable—that is, can be brought into bistable regime only by recurrent excitatory synaptic inputs.

The collective network dynamics depends on a and other parameters such as the excitatory coupling strength W_E . Such a *state diagram* (the network behavior as function of a and W_E) is shown in Fig. 7. In order for the uniform rest state to exist and be stable, W_E should be below a critical line (solid curve). At higher W_E values, this Down state is destabilized by strong recurrent excitations. If W_E is too large (above the dashed line), the stable uniform Up state exists, which cannot be used to encode the cue position. On the other hand, if W_E is too small (below the dotted curve), the excitatory reverberations are not powerful enough to sustain a nonuniform activity profile. Therefore, W_E should be limited between the dotted curve and the solid curve; too large or too small W_E would disrupt the normal working memory function of the network model.

To conclude, normal working memory function of the network model is based on the coexistence between a low spontaneous state and nonuniform profiles. This depends on an interplay between intrinsic cell properties and synaptic connections and requires that both a and W_E be limited within certain ranges: $a_1 < a < a_2$, and W_E between the dotted and solid curves in Fig. 7.

When the (a, W_E) values are close to one of these four curves in Fig. 7, the quantitative properties of the

nonuniform activity profiles are changed as follows. First, as a is decreased toward a_1 , the profiles become narrower, and the maximal firing rate becomes unrealistically small (although the gap, given by $r_+ - r_-$ (cf. Fig. 1A), never becomes zero). As a consequence, the memory storage of the cue position is not robust against noise. Second, as a is increased above a_2 , there is still a coexistence of a stable Down state and a Profile state. However, the network’s ability to hold the profile is not due exclusively to the recurrent excitations, since all the cells in the network are in the bistable regime (I_1 is now below zero). Consequently, the widths of the profiles become unrealistically large, and Gaussian fits for tuning curves are no longer possible. Third, as W_E is increased across the dotted curve, there is a discontinuous transition for the emergence of Profile states with a finite width and gap. For W_E slightly above the dotted line, a is the dominant factor in shaping the form of the profile, while the synaptic parameters control the ability for the network to sustain such a profile. Finally, for W_E above the solid curve, the Down state is no longer stable, and the only stable behaviors are nonuniform profile states. Note that, in fact, Profile states can exist even in the absence of intrinsic conditional bistability ($a < a_1 = 0.3376$), in which case the activity profiles are smooth without gaps. However, they do not coexist with a stable resting state and hence cannot be used for working memory storage. We show below that, in a different regime of model parameters, network bistability between a rest state and active profile states is possible without intrinsic conditional bistability of single neurons.

We also considered the state diagram on the (W_E, W_I) plane (Fig. 8). Again, the coexistence between a resting state and active profile states requires that W_E be between the dotted and solid curves. The most noticeable feature of this diagram is that the dotted and solid curves run somewhat in parallel along the diagonal line. That is, more powerful excitation needs to be controlled by stronger inhibition, and vice versa; a balance between synaptic excitation and inhibition is required for working memory function of the network model.

We can see from Fig. 8 that the stronger the inhibitory coupling strength W_I , the narrower the range for W_E between the dotted and solid curves. Synaptic inhibition also modulates strongly the shape of tuning curves and thus the neuronal memory fields: stronger inhibition leads to narrower tuning and smaller maximum firing rate (Fig. 9). Note that as the profile width

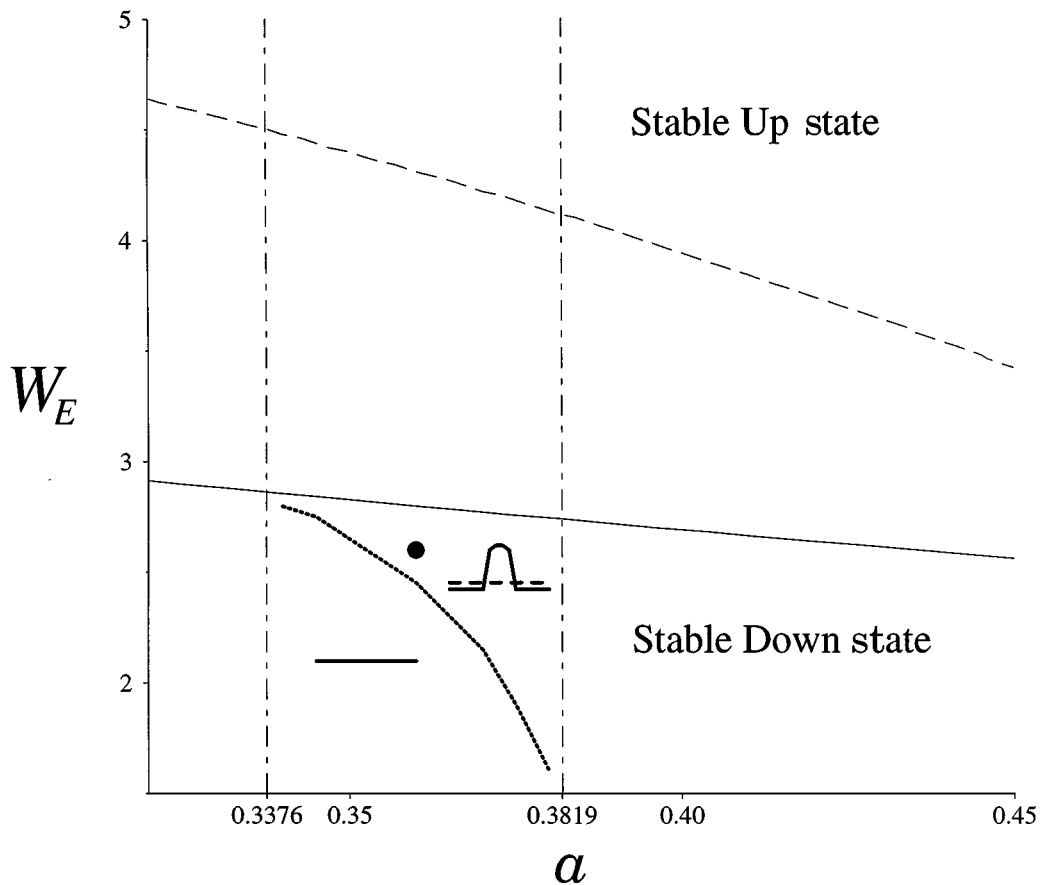


Figure 7. State diagram of the network model on the two-dimensional plane corresponding to the cellular parameter a and the synaptic parameter W_E . There are three types of steady states: Down state (the resting state), Up state (a uniformly excited state), and Profile states (a continuum of nonuniform activity patterns). The Down state is stable below the solid line and becomes unstable above it. The stable Up state emerges above the dashed curve. The Profile states exist only above the dotted curve. Between the solid and dotted curves, nonuniform profiles coexist with a stable resting state of spontaneous activity, which is required for the working memory storage by the network. The reference parameter set (in the Methods section) is indicated by a filled circle. The limiting cases for the single-cell input-output relation are indicated by the two vertical dot-dashed lines (see text for discussions).

increases (corresponding to smaller W_I), the tuning curves are wider, and their fit to Gaussian curves becomes unsatisfactory. This is due to the fact that more neurons are in the upper level of activity in the profile state.

Local Change in Parameters

In a large neural population, the behavior of each individual neuron is determined by the convergent action from all other cells in the network. Therefore, local changes of either intrinsic properties or synaptic strengths in one or a few cells should modify only the tuning curves of the affected cells but not those of other neurons. This was shown in simulations, where

the synaptic parameter W_E or intrinsic parameter a was decreased for a single cell (Figs. 10B and 10C, respectively). The manipulations reduced the neuronal excitability and the width of its memory field, compared to control (Fig. 10A). However, other cells in the population are not affected. The network activity profile remains the same except for the affected cell (data not shown). Conversely, an increase in either of the two parameters could selectively enhance the tuning curve of the affected cell.

Memory Fields Without Cellular Bistability

Until now, we have assumed that PFC neurons exhibit intrinsic conditional bistability. On the other hand,

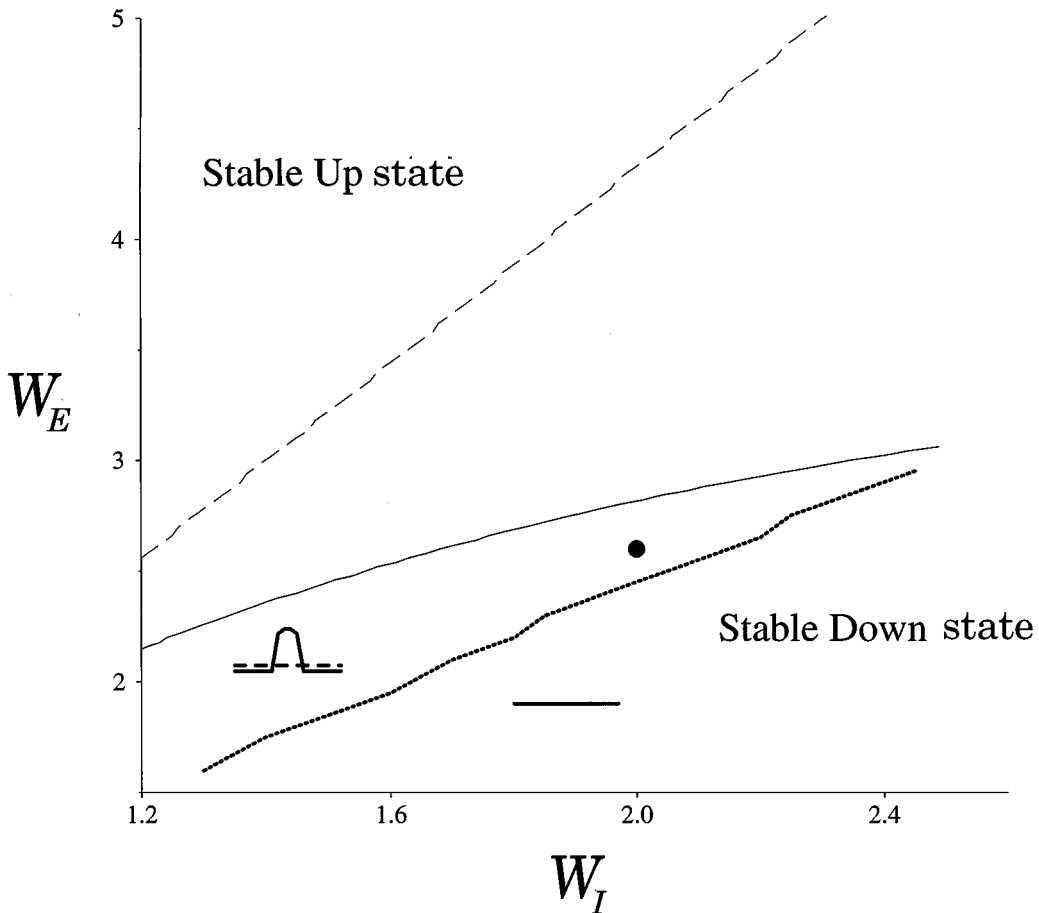


Figure 8. State diagram as function of W_I and W_E . Coexistence of a stable rest state and nonuniform activity profiles requires a rough balance between recurrent synaptic excitation and inhibition, as seen by the diagonal shapes of the curves. Same symbol and line conventions as in Fig. 7.

activity patterns that coexist with the rest or Down state can arise as a network dynamical property, even when bistability is not present at the single-cell level (see, for example, Amari, 1977; Wilson and Cowan, 1973). Thus, it is important to investigate which of the results reported above relies on intrinsic bistability. This can be achieved by modifying our model in two possible ways. On the one hand, a can be chosen to be smaller than $a_1 = 0.3376$, in which case the input-output relation loses its S-shape and becomes monostable (Fig. 11A). Alternatively, we can let $a = 0$, $b = 0$, and $c = 0$ in $f(r)$ (cf. Eq. (2)), so that Eq. (1) is reduced to $\tau_0 dr/dt = -r + g(I)$. In this case, the gain function $g(I)$ (which is also the input-output relation $r = g(I)$) is changed to acquire a nonlinear form (Fig. 11B). Both modifications yield an input-output relation of the

sigmoid type. There is no intrinsic conditional bistability, but the network working memory behavior described below does depend crucially on properties of this single cell input-output relation. In particular, the slope of the curve (the gain) should be sufficiently large within a certain input range.

In model simulations, we found that memory fields could be realized using either of the two kinds of input-output relations described above. In what follows, we shall limit ourselves to the second case, with $a = b = c = 0$ and $g(I)$ being a piece-wise linear function (Fig. 11B). Note that the slope of $g(I)$ between I_1 and I_2 is twice as large as in Fig. 1B.

Figure 12 shows a network profile of persistent activity and the tuning curve for a single neuron, obtained using the same simulation protocols as in Figs. 3 to 5.

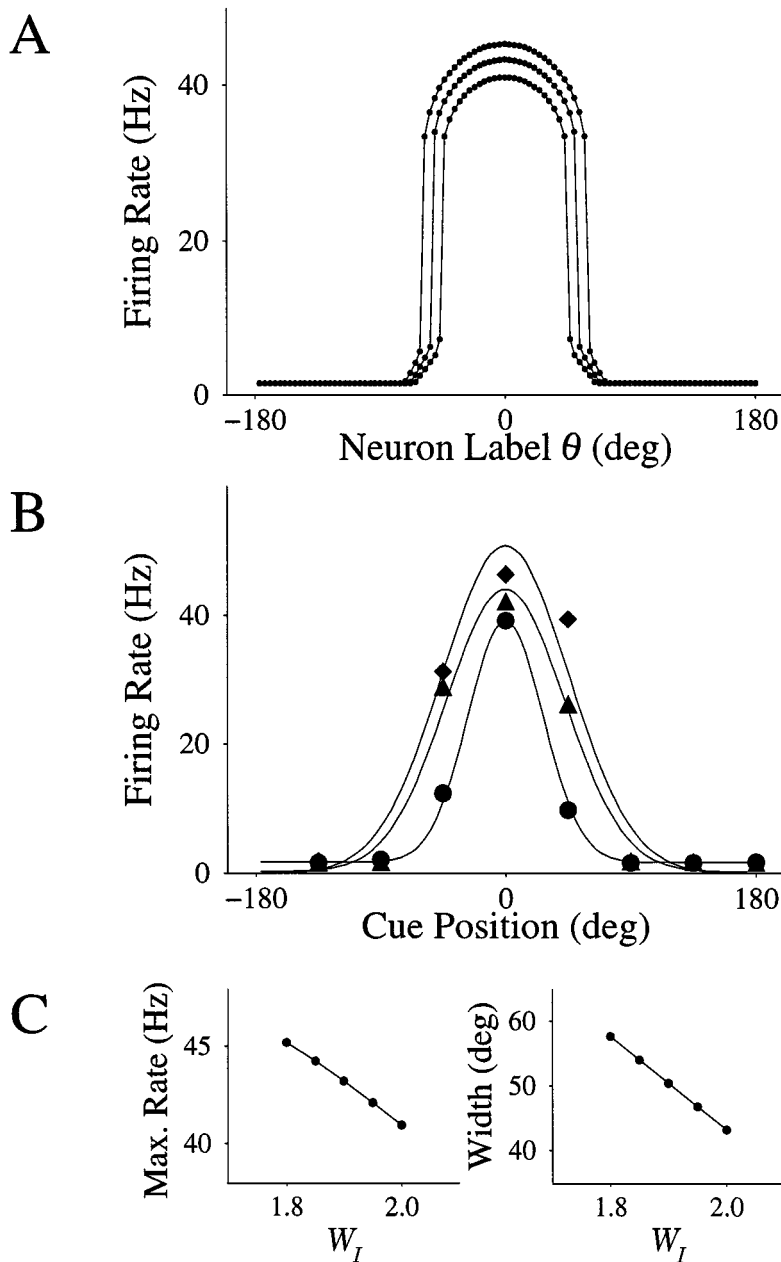


Figure 9. The widths of activity profiles and tuning curves are modulated by the synaptic inhibition strength. A: Network activity profiles obtained with three different values of W_I . Wider profiles correspond to smaller W_I values. B: Tuning curves for the cell at $\theta = 0$ degree with the same three W_I values as in A. The Gaussian widths are 27.06, 42.55, and 45.59 degrees, respectively. C: The width of activity profile (right panel) and the peak firing rate (left panel), as function of W_I . A network activity profile with gaps cannot be fitted by Gaussian curves, in which case its width is defined as half the angular size of the upper plateau. No noise was present for simulations in panels A and C.

In contrast with the case where single cells are conditionally bistable, here the activity profile is continuous and smooth (Fig. 12A). In the absence of gaps, tuning curves appear to be wider; a larger exponent q

(cf. Eq. (5)) was used so that the excitatory connections were more localized, and the tuning curve (Fig. 12B) remained comparable with the experimental data of Funahashi et al. (1989).

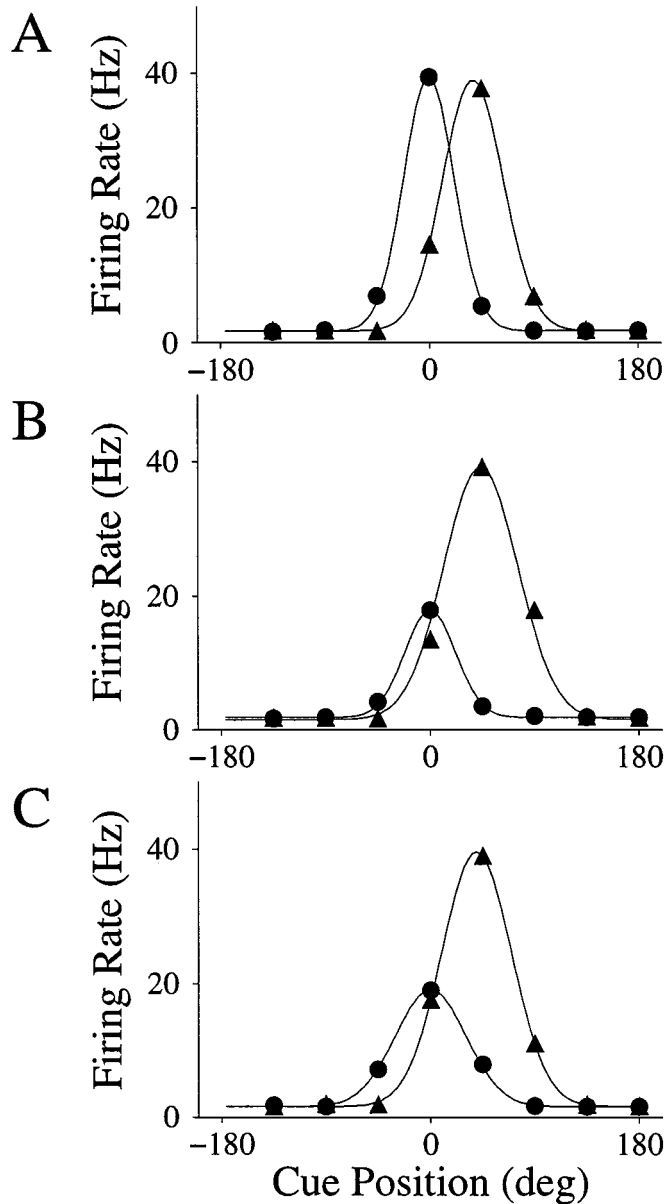


Figure 10. Effect of local modulation of synaptic excitation or intrinsic neuron properties. (A) Control: tuning curves for neurons with memory field at $\theta = 0$ degree (circles) and at $\theta = 45$ degrees (triangles), respectively, together with their best Gaussian fits. The excitatory synaptic parameter W_E is decreased from 2.6 to 2.26 (B), or the intrinsic parameter a is decreased from 0.36 to 0.335 (C), only for the cell at $\theta = 0$ degree, in both cases, the reduction of persistent activity of the affected cell is selective. The tuning curves of other cells, such as the one at $\theta = 45$ degrees, remain unaltered.

Can the two models with and without cellular bistability be distinguished by existing data and future experimental tests? Tuning curves calculated with eight cue locations do not allow us to distinguish between a smooth profile and a discontinuous one with gaps. Furthermore, gaps can be averaged out with noise

(see Fig. 4A). However, given a cue, the predicted *distribution* of firing rates of delay-period activity across the neural population is significantly different for the two models: it shows a much more conspicuous bimodality in the presence of cellular bistability, when there are very few cells with firing rates intermediate

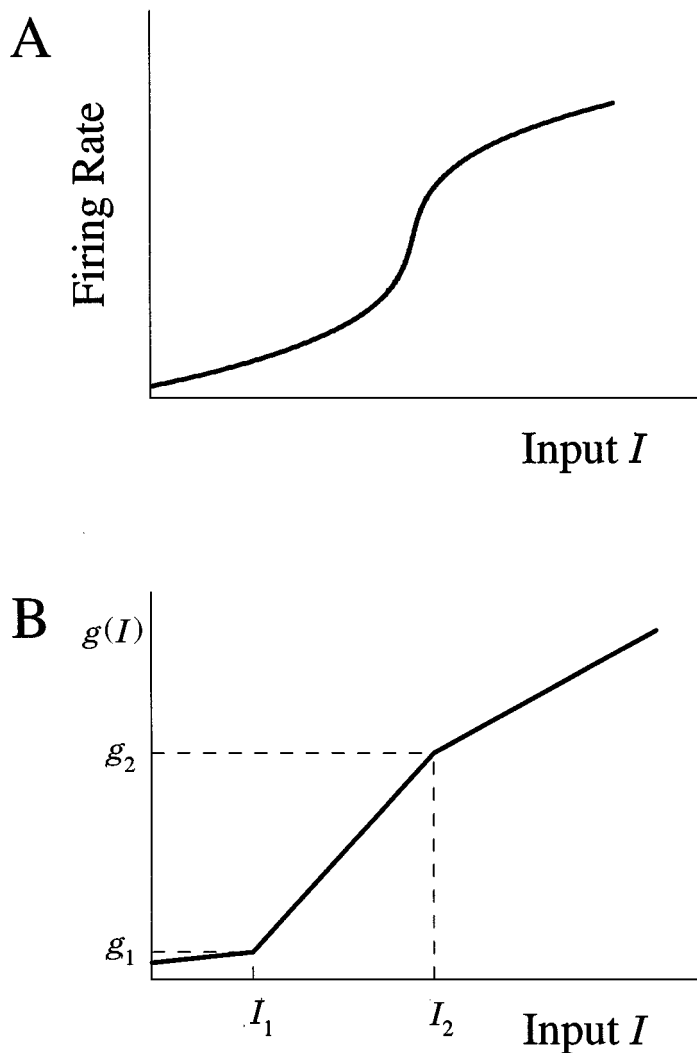


Figure 11. A: Single-cell input-output relation for Eqs. (1) and (2) without cellular bistability ($a = 0.33 < a_1$, cf. Fig. 7). B: Modified gain function $g(I)$, used in the case with $a = b = c = 0$. The parameters are $g_1 = 0.5$, $g_2 = 4.1$, $I_1 = 1$, and $I_2 = 2.8$, so that the slope between I_1 and I_2 is 2. The slope of the function is 0.2 below I_1 , and 1.0 above I_2 . Notice the sigmoidal character of both curves, a necessary condition for the emergence of network activity profiles that coexist with a stable rest state, in the absence of bistability at the single-cell level.

between the active and inactive neural groups (Fig. 13). Note that the rate distribution can be bimodal even without cellular bistability, if the input-output curve $r = g(I)$ is sufficiently steep near the threshold (such as a step function) so that there is an effective gap between the firing rates of the active and inactive states. However, this situation occurs only if the middle branch of $g(I)$ is almost vertical in Fig. 11B, and thus the neuron is nearly bistable (it becomes truly bistable when the middle slope is negative).

Furthermore, we found that the *temporal dynamics* of the network persistent activity is quite different

between the two models, especially in their respective ability to sustain the working memory of the cue position against noise or a distraction.

Noise-Induced Drift

How well the model can retain an accurate memory of cue information depends on its ability to keep its peak activity localized near the neurons whose memory field represent the cue location, even in the presence of noise. In other words, we should determine whether the cue position, network-encoded by the population

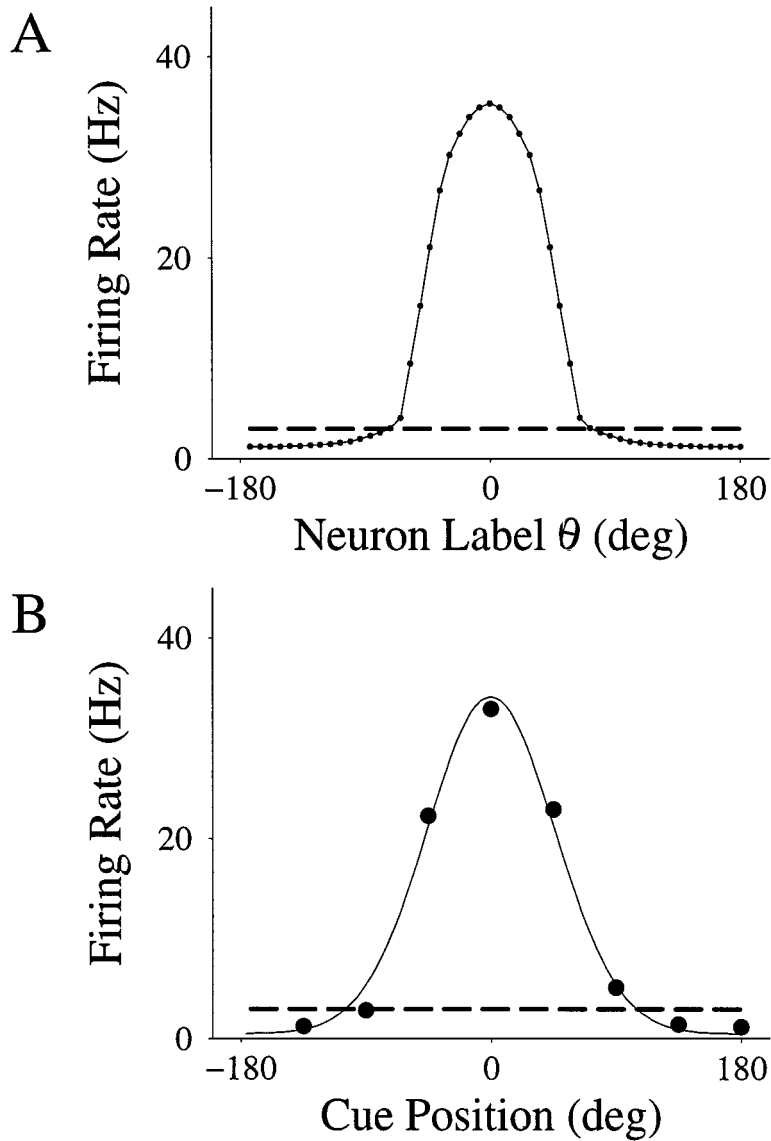


Figure 12. A: Steady-state profile of the persistent network activity during delay period, for the model without intrinsic bistability (using $f(r) = r$ and the modified gain function of Fig. 11B). In this case, a larger excitation/inhibition ratio (W_E/W_I) is needed for the maintenance of an active profile. In contrast to Fig. 4A, here the profile is smooth without gaps. B: The corresponding tuning curve (with best Gaussian fit) for the neuron at $\theta = 0$ degree. The Gaussian width of the tuning curve is 46 degrees. (Other parameters are $W_I = 1$, $W_E = 5$, $p = 1$, $q = 6$, and $I_0 = 0.6$.)

vector (θ_{peak} , Eq. (9)), stays close to the actual cue position θ_{cue} over time, in spite of random noise perturbations. We performed simulations to address this question for both models (Fig. 14). (Note that, since a limited number of neurons were used in the simulations, the noise should be viewed as being locally coherent.) If $q = 1$ (cf. Eq. (5)) for both versions of the model, the activity profile is wider without cellular bistability, and the time courses of θ_{peak} are

dramatically different for the two models (Fig. 14, top and middle panels). The network endowed with intrinsic conditional bistability is able to stabilize θ_{peak} near θ_{cue} for a long time. By contrast, the network with only sigmoid cellular input-output relation displays a significant random drift in θ_{peak} , which increases in amplitude with time and reaches up to ± 30 degrees away from θ_{cue} within 5 to 10 s (comparable to delay-period durations). Clearly, the effect is partly caused by the difference in

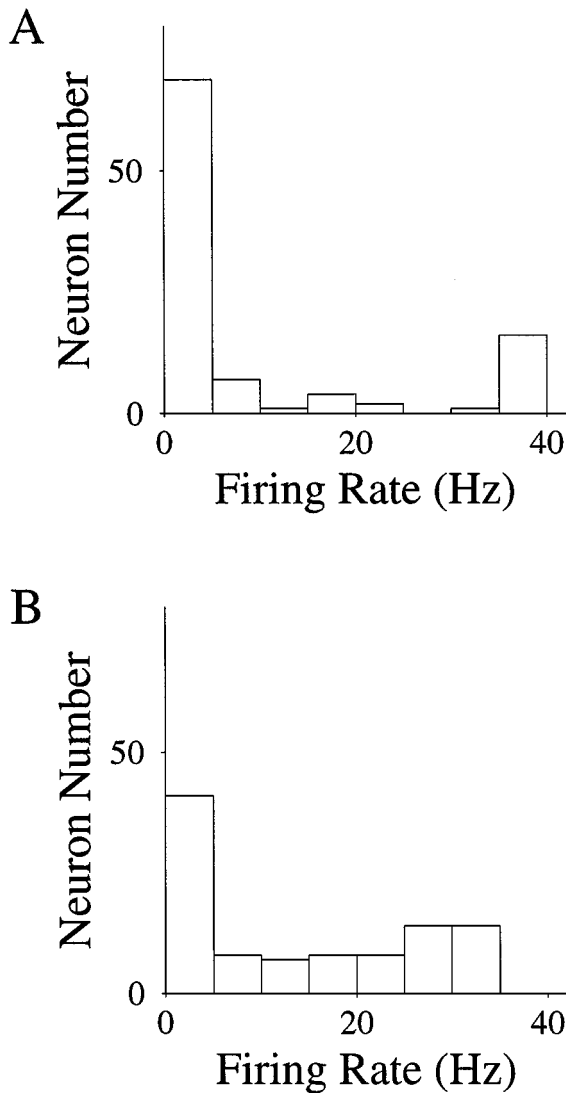


Figure 13. Distribution of firing rates during delay-period activity across the neural population with cellular conditional bistability (A) and without it (B). There is a much clearer bimodality in panel A than in panel B. The simulation was done with a network of 100 neurons; parameters as in Figs. 3 and 12, respectively; noise present in simulations.

the activity profile tuning. We also simulated the model without intrinsic bistability using $q = 6$. As expected, the network with a narrower activity profile ($q = 6$ versus $q = 1$) shows less noise-induced drift (Fig. 14, middle and lower panels). However, given that the two model versions display comparable activity profiles, we can see that with cellular bistability the network is still much more robust against noise-induced drift (Fig. 14, upper and lower panels).

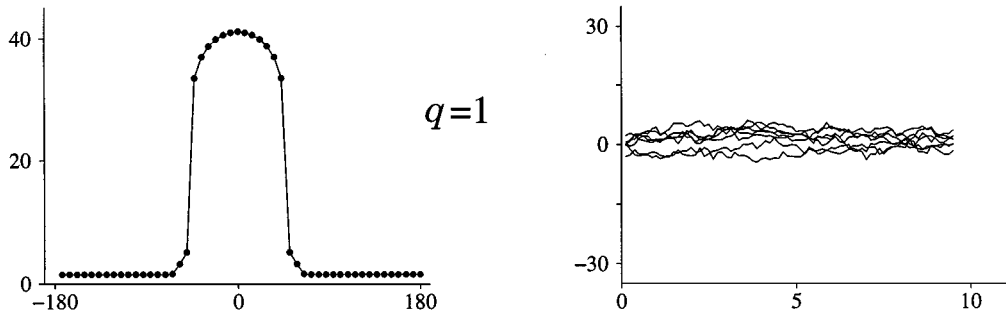
The strikingly different behaviors of the two models originate in the presence or absence of gaps in the network activity profile. If single cells are conditionally bistable, the gaps act to “protect” the memory of the cue position against noise: to perturb this memory by effectively moving the peak of the profile to another position, perturbations must be locally coherent and sufficiently large to overcome the barrier across a finite gap, otherwise an inactive cell could not be brought up to the excited state or an active cell be switched down to the rest state. By contrast, in the model without intrinsic bistability there are no gaps in the activity profile. Thus small (but locally coherent) perturbations can move the profile slightly. This leads to random diffusion of the encoded cue position θ_{peak} , as seen in Fig. 14.

Distraction Simulation

Another manipulation to assess the robustness of the model performance is to observe its response to a distraction stimulus—that is, a second cue input presented transiently during the delay period at a location different from the first cue. Would the network preserve the memory of the first cue, or would it be perturbed and thereafter “remember” a wrong cue position?

Figure 15 shows the results of a distraction simulation with both versions of the model. The first cue position is located at $\theta_{\text{cue}} = 0^\circ$. A second stimulus is presented during the delay period, with a cue identical in size and duration to the first one but at different positions ($\theta_{\text{distractor}} = 45, 90,$ and 135 degrees, top to bottom panels). Noise is present in these simulations but with a smaller amplitude than in Fig. 14, so that the noise-induced drift does not interfere with the distraction effect (the effect is still present with a higher level of noise, but its visualization is more difficult). We observed that in the model with cellular conditional bistability (Fig. 15, left panels), the population-vector coded cue position θ_{peak} is somewhat perturbed by the distraction but remains much closer to the original cue position θ_{cue} than to $\theta_{\text{distractor}}$. Again, the robustness against distraction is related to the presence of gaps in the activity profile, as with the noise-induced drift effect. Moreover, the shift $\theta_{\text{peak}} - \theta_{\text{cue}}$ is not significant when $\theta_{\text{distractor}}$ is far away from θ_{cue} (left bottom panel). This is because cells at large distances away from θ_{cue} are strongly inhibited by active cells. Therefore, these cells are less likely to be excited and switched on by the distraction stimulus, even if the latter is of the same

Model with Intrinsic Bistability



Model without Intrinsic Bistability

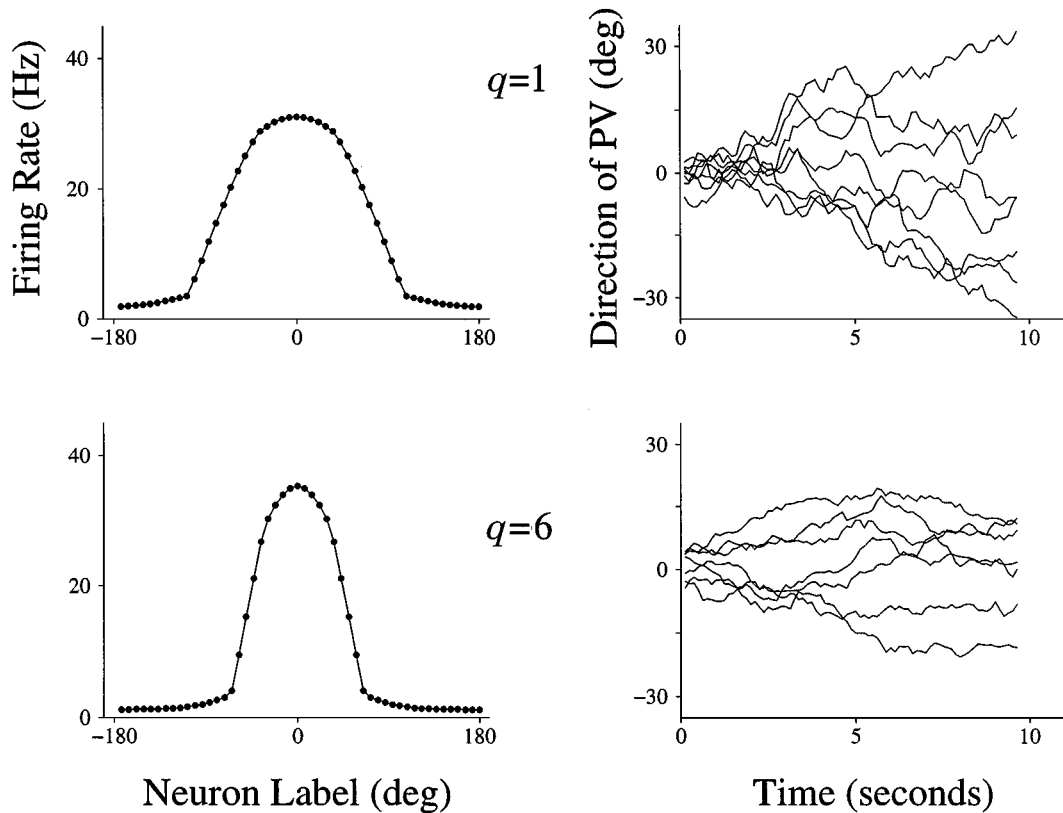


Figure 14. Noise-induced drift in the cue position encoded by the population vector (θ_{peak} , cf. Eq. (9)), during delay period. The cue position was at $\theta = 0$ degree, and data were recorded starting right after the transient cue. Left panels show activity profiles, while right panels show the corresponding noisy time evolutions of θ_{peak} . The top panels correspond to the model endowed with intrinsic bistability, using $q = 1$ ($W_I = 2$, $W_E = 2.6$). The middle and bottom panels correspond to the model without intrinsic bistability, with $q = 1$ and $q = 6$, respectively. We note that the drift is always significant without cellular bistability, although the effect is somewhat diminished if q is larger (and hence the profile more sharply tuned). The top and bottom panels compare the two models with similar activity profiles, the noise-induced drift is still much smaller in the model with intrinsic bistability, due to the presence of gaps in its activity profile ($W_I = 1$; $W_E = 2.9$ for $q = 1$ and 5 for $q = 6$).

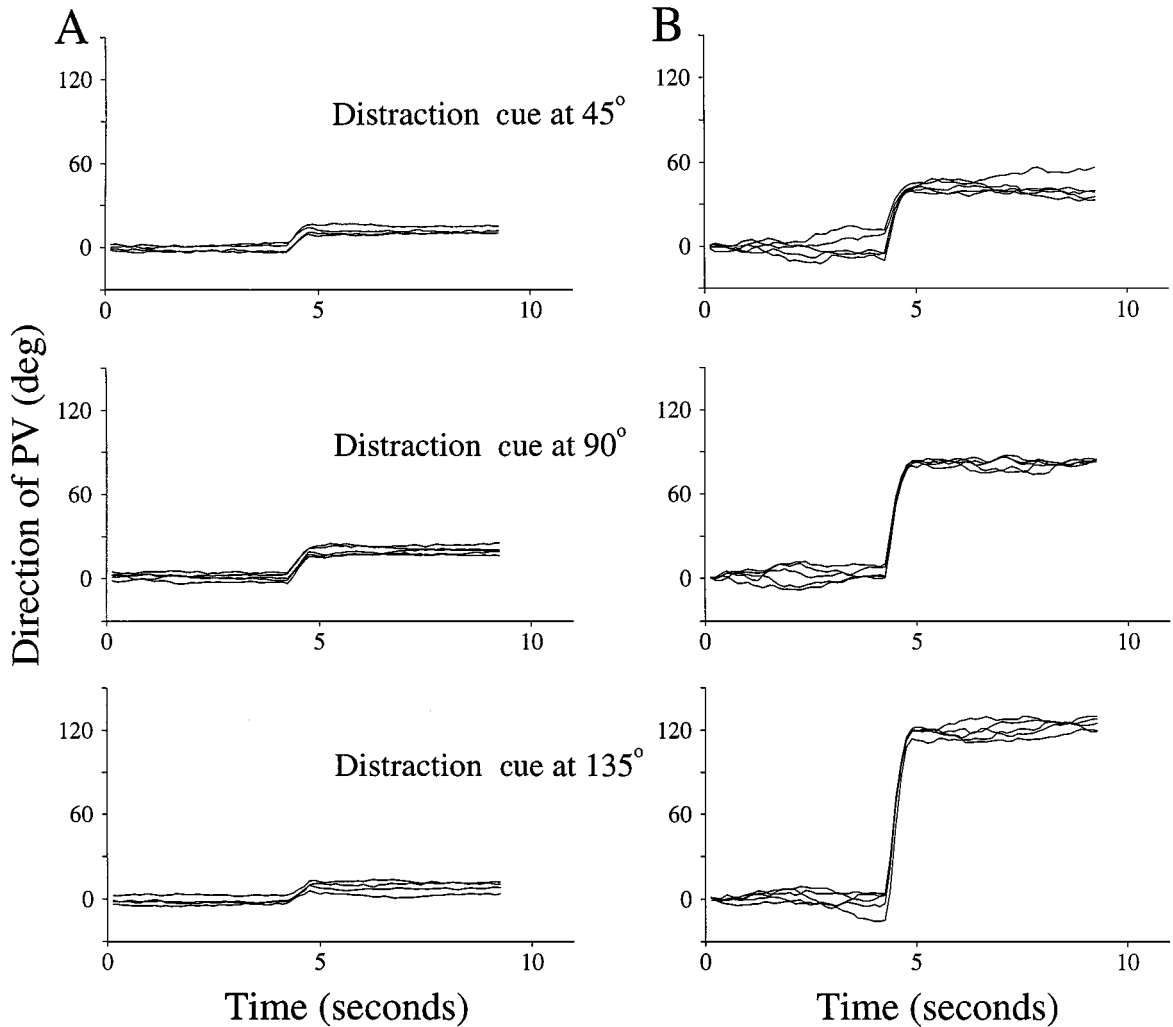


Figure 15. Simulated distraction experiment for a network model with or without cellular bistability (panels A and B, respectively), in the same setup as that for Fig. 14. At $t \simeq 4.5$ s into the delay period, a distraction stimulus, equal in strength and duration to the original cue, was presented at 45, 90, or 135 degrees. The time evolution of the population-vector encoded cue position, θ_{peak} , is plotted in each case (top to bottom panels, respectively). In the presence of cellular bistability (A), the working memory storage is reliable against distractions. This is in striking contrast to the situation in (B), where systematic shifts in θ_{peak} are produced by the distraction stimuli. ($q = 1$ for both models.)

amplitude and time duration as the first cue stimulus. By contrast, in the model without cellular bistability, distraction is very effective, and the farther away $\theta_{\text{distractor}}$ is from θ_{cue} , the larger is the shift (Fig. 15, right panels). After the distraction, the population-vector coded cue position θ_{peak} becomes very close to $\theta_{\text{distractor}}$ in all three cases; thus, the memory about the original cue position is completely lost.

Discussion

The present computational work is based on the premise that the persistent activity observed dur-

ing oculomotor delayed-response experiments of Funahashi et al. is generated locally within the the dorso-lateral PFC. The PFC carries out working memory tasks in interplay with multiple cortical regions. Indeed, delay-period persistent activity has also been observed in other cortical areas that are involved in the particular tasks, such as neurons in the posterior parietal cortex during visuospatial experiments (Gnadt and Andersen, 1988; Chafee and Goldman-Rakic, 1998) or in the inferior-temporal cortex during object delayed-response experiments (Miyashita and Chang, 1988; Miller et al., 1993). An important question is whether such mnemonic neuronal activity is generated locally

within each cortical area. Recent experiments, using a protocol similar to our distraction simulation, indicate that the PFC may be at the origin of the persistent activity observed in the parietal and inferior-temporal cortices. In a delayed match-to-sample experiment, nonmatch (distraction) stimuli were presented between the sample and match stimuli. Persistent activity recorded from inferior temporal cortex (Miller et al., 1993) or from posterior parietal cortex (Constantinidis and Steinmetz, 1996) was found to be abolished immediately after the first nonmatch stimulus; whereas the monkey's behavioral performance was not affected. By contrast, sustained activity of the PFC cells was found to persist in the presence of the intervening stimuli (Miller et al., 1996). These data suggest that the PFC network alone should be capable of forming the memory fields of its constituent neurons, which subserve the neuronal basis of active working memory. Nevertheless, further experiments need to be carried out in order to determine the precise roles of the reciprocal interaction loops between the PFC and sensory cortical areas, in the working memory storage and online information manipulation.

In the model, we used a simple circuit connectivity with localized feedback excitation and more widespread inhibition, adapted from Ben-Yishai et al. (1995). Such a network architecture is consistent with known PFC circuit properties (Levitt et al., 1993; Kritzer and Goldman-Rakic, 1995). Our model, however, does not assume inhibitory synaptic connections that are specific to cross-orientation columns (Goldman-Rakic, 1995). We postulate that working memory of visuospatial cues is stored in the form of a *continuum* of network activity profiles, as distributed population code of graded cue location, which coexist with a uniform state of spontaneous activity. Under these assumptions, we investigated whether a pure network mechanism (Wilson and Cowan, 1973; Amari, 1977) was sufficient to reproduce the observations of Funahashi et al. (1989) and whether the network model would behave differently if single neurons were endowed with cellular bistability (presumably due to intrinsic ion channel mechanisms). Note that, unlike in Guigon et al. (1995), we did not assume that single cells are bistable devices by themselves. Rather, bistability is *conditional* and requires sustained synaptic inputs originating from the network. We found that, in principle, memory fields of neuronal delay-period activity could be constructed with or without cellular bistability. Note that, even in the latter case, the formation of memory fields does depend on the single cell's input-output relation, especially its sufficiently

large slope (gain) within an intermediate input range (Fig. 11). Therefore, in principle network behavior can be altered through modulation of intrinsic cellular characteristics.

Because of the spatial translational invariance of activity profiles, noise or distraction stimuli could, in the absence of cellular bistability, induce systematic drifts over time of the population-vector coded cue position, so that the memory would be lost after a few seconds. The drifts are less likely if there is a gap between the firing rates of inactive and active cells, which can be overcome only by (infrequent) noise perturbations of large amplitudes (Fig. 14). Such a gap is naturally realized if single neurons are bistable with an input-output relation like in Fig. 1A. If the input-output curve is monotonic but very steep (almost vertical) near the input threshold, the lower (inactive) and upper (active) branches will also be separated by an apparent discontinuity. This situation, however, is biologically unplausible *unless* single neurons are close to be bistable. Thus, our results suggest that cellular bistability represents a candidate neuronal contribution to the robust working memory performance of the PFC network. Other (synaptic) mechanisms are conceivable and will be investigated in future studies.

Can cellular bistability or its absence be assessed using extracellular recording data from PFC cells of the awake behaving monkey? Our results suggest two testable predictions. One is based on the observation that a cell with cellular bistability could be induced by noise to switch randomly between a low spontaneously firing state and a highly excited state, and switching is expected to be more frequent for cue position located intermediately between the cell's best and worst stimuli (cf. Fig. 4). The other prediction is that for a given cue stimulus, the distribution of firing rates of delay period activity across neural pools should be clearly bimodal if single cells are conditionally bistable (Fig. 13). On the other hand, the question of whether PFC neurons are capable of intrinsic bistability can be addressed by *in vitro* intracellular recordings. To detect *conditional* bistability, brief current pulses should be applied to the cell that is superimposed on a tonic current level of appropriate intensity (cf. Fig. 1C). Such a stimulation protocol has not been reported in previous studies using rat PFC slices (Gejjo-Barriento and Pastore, 1995; Hammond and Crépel, 1992; Yang and Seamans, 1996). It is also not known how PFC cell electrophysiology may differ between rodents and primates. Moreover, it is likely that bistability at the single neuron level may depend on neuromodulatory inputs (Kiehn, 1991; Marder et al., 1996), hence, it would be observable in

slices only when certain transmitter receptors are activated pharmacologically. For instance, acetylcholine, serotonin, and norepinephrine are potent inhibitors of a Ca^{2+} -dependent K^+ current (I_{AHP}) and a voltage-gated M-type K^+ current (I_{M}) (Madison et al., 1987; McCormick and Williamson, 1989). The blockade of I_{AHP} and I_{M} could unmask a calcium plateau potential that, if sufficiently large, could give rise to bistability (Kiehn, 1991; Booth et al., 1997). In addition, muscarinic activation of a Ca^{2+} -gated nonselective cation current (I_{Can}) (Haj-Dahmane and Andreda, 1996) could also contribute to such bistability phenomenon.

The prefrontal cortex is a major target of the brainstem dopamine afferents, and several investigations have suggested a link between dopamine receptors and working memory in the PFC (Goldman-Rakic, 1995; Williams and Goldman-Rakic, 1995). For example, Sawaguchi and Goldman-Rakic (1991) found that D1 antagonists impaired memory-guided saccades for specific targets that varied with the site of drug injection. This modulatory effect can be very selective and limited to individual neurons (Williams and Goldman-Rakic, 1995). The action of dopamine in the PFC is complex, through multiple pathways involving both intrinsic ion currents (Gejjo-Barriento and Pastore, 1995; Yang and Seamans, 1996) and synaptic transmissions (Cépeda et al., 1992). Motivated by these observations, we performed model simulations where either an intrinsic cell parameter (a) or the excitatory synaptic strength (W_E) is reduced locally in a single cell. Similarly to the findings of Williams and Goldman-Rakic (1995), we found that local modulation affects the cell's response to its preferred cue stimuli but not responses to other cue stimuli or its spontaneous firing rate (Fig. 10). Moreover, the tuning curves of other cells remain the same because changes in a single cell (or a few cells) cannot influence substantially the memory fields of other cells that are generated by collective dynamics in a large neuronal assembly. It is also relevant to note that, if parameters are varied globally, there is an optimal combination of intrinsic cell properties and synaptic recurrent connections for the working memory function of the network model (Figs. 7 and 8). How these simulation results may be related to the dopamine modulation of the memory fields of PFC cells remains to be explored in future studies.

The simple firing-rate model presented in this work can be improved and extended in several respects. First, a biologically more realistic model can be constructed, using spiking neurons, two (excitatory and inhibitory)

populations of cells, and synaptic currents with realistic gating kinetics. Second, more detailed anatomical data about the PFC circuit (Levitt et al., 1993; Kritzer and Goldman-Rakic, 1995) needs to be taken into account. Third, Hebbian synaptic plasticity has been studied in models where memory items for objects are stored by a *discrete* number of firing pattern attractors (Zipser et al., 1993; Guigon et al., 1995; Amit et al., 1994; Amit and Brunel, 1997). In the case of visuospatial memory, a *continuum* of activity profiles (or a large number of discrete attractors with approximate spatially translational symmetry) need to be stored. How this can be achieved through Hebbian learning mechanisms remains to be investigated in future research.

Acknowledgments

We thank Drs. P. Goldman-Rakic and E. Marder for valuable discussions and encouragement. This work was supported by the Alfred P. Sloan Foundation, the Office of Naval Research, and the W.M. Keck Foundation.

References

- Amari S (1977) Dynamics of pattern formation in lateral-inhibition type neural fields. *Biological Cybernetics* 27:77–87.
- Amit DJ, Brunel N (1997) Model of global spontaneous activity and local structured activity during delay periods in the cerebral cortex. *Cereb. Cortex* 7:237–252.
- Amit DJ, Brunel N, Tsodyks MV (1994) Correlations of cortical Hebbian reverberations: Experiment versus theory. *J. Neurosci.* 14:6435–6445.
- Ben-Yishai R, Hansel D, Sompolinsky H (1997) Traveling waves and the processing of weakly tuned inputs in a cortical network module. *J. Comput. Neurosci.* 4:57–77.
- Ben-Yishai R, Lev Bar-Or R, Sompolinsky H (1995) Theory of orientation tuning in visual cortex. *Proc. Natl. Acad. Sci. USA* 92:3844–3848.
- Booth V, Rinzel J (1995) A minimal, compartmental model for a dendritic origin of bistability of motoneuron firing patterns. *J. Comp. Neurosci.* 2:1–14.
- Booth V, Rinzel J, Kiehn O (1997) A compartmental model of vertebrate motoneurons for Ca^{2+} -dependent spike and plateau potentials under pharmacological treatment. *J. Neurophysiol.* 78:3371–3385.
- Camperi M, Wang X-J (1997) Modeling delay-period activity in the prefrontal cortex during working memory tasks. In: JM Bower, ed. *Computational Neuroscience: Trends in Research*, 1997. Plenum Press, pp. 273–279.
- Cépeda C, Radisavljevic Z, Peacock W, Levine MS, Buchwald NA (1992) Differential modulation by dopamine of responses evoked

- by excitatory amino acids in human cortex. *Synapse* 11:330–341.
- Chafee MV, Goldman-Rakic PS (1998) Neuronal activity in macaque prefrontal area 8a and posterior parietal area 7ip related to memory guided saccades. *J. Neurophysiol.* 79:2919–2940.
- Cohen JD, Perlstein WM, Braver TS, Nystrom LE, Noll DC, Jonides J, Smith EE (1997) Temporal dynamics of brain activity during a working memory task. *Nature* 386:604–608.
- Constantinidis C, Steinmetz MA (1996) Neuronal activity in posterior parietal area 7a during the delay periods of a spatial memory task. *J. Neurophysiol.* 76:1352–1355.
- Courtney S, Ungerleider LG, Keil K, Haxby JV (1997) Transient and sustained activity in a distributed neural system for human working memory. *Nature* 386:608–611.
- Douglas RJ, Martin KAC, Whitteridge D (1991) A functional microcircuit for neocortex. *Neural Comput.* 1:480–488.
- Funahashi S, Bruce CJ, Goldman-Rakic P (1989) Mnemonic coding of visual space in the monkey's dorsolateral prefrontal cortex. *J. Neurophysiol.* 61:331–349.
- Fuster J (1988) *The Prefrontal Cortex* (2nd ed.). Raven, New York.
- Fuster J, Alexander G (1971) Neuron activity related to short-term memory. *Science* 173:652–654.
- Geijo-Barriento E, Pastore C (1995) The effects of dopamine on the subthreshold electrophysiological responses of rat prefrontal cortex neurons in vitro. *Euro. J. Neurosci.* 7:358–366.
- Georgopoulos AP, Schwartz A, Kettner RE (1986) Neuronal population coding of movement direction. *Science* 233:1416–1419.
- Gilbert CD (1993) Circuitry, architecture, and functional dynamics of visual cortex. *Cereb. Cortex* 3:373–386.
- Gnadt JW, Andersen RA (1988) Memory related motor planning activity in posterior parietal cortex of macaque. *Exp. Brain Res.* 70:216–220.
- Goldman-Rakic P (1987) Circuitry of the prefrontal cortex and the regulation of behavior by representational knowledge. In: F Plum, V Mountcastle, eds. *Handbook of Physiology*. American Physiological Society, Bethesda, MD. pp. 373–417.
- Goldman-Rakic P (1995) Cellular basis of working memory. *Neuron* 14:477–485.
- Guigon E, Dorizzi B, Burnod Y, Schultz W (1995) Neural correlates of learning in the prefrontal cortex of the monkey: A predictive model. *Cereb. Cortex* 2:135–147.
- Haj-Dahmane S, Andreda R (1996) Muscarinic activation of a voltage-dependent cation non-selective current in rat association cortex. *J. Neurosci.* 16:3848–3861.
- Hammond C, Crépel F (1992) Evidence for a slowly inactivating K^+ current in prefrontal cortical cells. *Euro. J. Neurosci.* 4:1087–1092.
- Haxby JV, Ungerleider LG, Horwitz B, Rapoport SI, Grady CL (1995) Hemispheric differences in neural systems for face working memory: A PET xCBF study. *Hum. Brain Mapp.* 3:68–82.
- Kiehn O (1991) Plateau potentials and active integration in the “final common pathway” for motor behavior. *Trends in Neurosci.* 14:68–73.
- Kritzer MF, Goldman-Rakic PS (1995) Intrinsic circuit organization of the major layers and sublayers of the dorsolateral prefrontal cortex in the rhesus monkey. *J. Comp. Neurol.* 359:131–143.
- Kubota K, Niki H (1971) Prefrontal cortical unit activity and delayed alternation performance in monkeys. *J. Neurophysiol.* 34:337–347.
- Levitt B, Lewis DA, Yoshioka T, Lund J (1993) Topography of pyramidal neuron intrinsic connections in macaque monkey prefrontal cortex (areas 9 and 46). *J. Comp. Neurol.* 338:360–376.
- Lukashin AV, Amirikian BR, Mozhaev VL, Wilcox GL, Georgopoulos AP (1996) Modeling motor cortical operations by an attractor network of stochastic neurons. *Biol. Cybern.* 74:255–261.
- Madison DV, Lancaster B, Nicoll RA (1987) Voltage clamp analysis of cholinergic action in the hippocampus. *J. Neurosci.* 7:733–741.
- Marder E, Abbott L, Turrigiano G, Liu Z, Golowash J (1996) Memory from the dynamics of intrinsic membrane currents. *Proc. Natl. Acad. Sci. USA* 93:13482–13486.
- McCarthy G, Blamire AM, Puce A, Nobre AC, Bloch G, Hyder F, Goldman-Rakic PS, Shulman RG (1994) Functional magnetic resonance imaging of human prefrontal cortex activation during a spatial working memory task. *Proc. Natl. Acad. Sci. USA* 91:8690–8694.
- McCormick DA, Williamson A (1989) Convergence and divergence of neurotransmitter action in human cerebral cortex. *Proc. Natl. Acad. Sci. USA* 86:8098–8102.
- Miller EK, Erickson CA, Desimone R (1996) Neural mechanisms of visual working memory in prefrontal cortex of the macaque. *J. Neurosci.* 16:5154–5167.
- Miller EK, Li L, Desimone R (1993) Activity of neurons in anterior inferior temporal cortex during a short-term memory task. *J. Neurosci.* 13:1460–1478.
- Petrides ME, Alivisatos B, Evans AC, Meyer E (1993) Dissociation of human mid-dorsolateral from posterior dorsolateral frontal cortex in memory processes. *Proc. Natl. Acad. Sci. USA* 90:873–877.
- Salinas E, Abbott L (1996) A model of multiplicative neural responses in parietal cortex. *Proc. Natl. Acad. Sci. USA* 93:11956–11961.
- Sawaguchi T, Goldman-Rakic P (1991) D1 dopamine receptors in prefrontal cortex: Involvement in working memory. *Science* 251:947–950.
- Somers D, Nelson S, Sur M (1995) An emergent model of orientation selectivity in cat visual cortical simple cells. *J. Neurosci.* 15:5448–5465.
- Steinberg IZ (1988) Computer simulations of the effect of non-inactivating sodium channels on the electric behavior of excitable cells. *J. Theor. Biol.* 133:193–214.
- Stemmler M, Usher M, Niebur (1995) Lateral interactions in primary visual cortex: A model bridging physiology and psychophysics. *Science* 269:1877–1880.
- Williams G, Goldman-Rakic P (1995) Modulation of memory fields by dopamine D1 receptors in prefrontal cortex. *Nature* 376:572–575.
- Wilson H, Cowan J (1973) A mathematical theory of the functional dynamics of cortical and thalamic nervous tissue. *Kybernetik* 13:55–80.
- Yang CR, Seamans JK (1996) Dopamine D1 receptor actions in layer V–VI rat prefrontal cortex neurons in vitro: Modulation of dendritic-somatic signal integration. *J. Neurosci.* 16:1922–1935.
- Yang CR, Seamans JK, Gorelova N (1996) Electrophysiological and morphological properties of layer V–VI principal pyramidal cells in rat prefrontal cortex in vitro. *J. Neurosci.* 16:1904–1921.
- Zhang K (1996) Representation of spatial orientation by the intrinsic dynamics of head direction cell ensembles: A theory. *J. Neurosci.* 16:2112–2126.
- Zipser D, Kehoe B, Littlewort G, Fuster J (1993) A Spiking network of Short-term active memory. *J. Neurosci.* 13:3406–3420.